ECS Transactions, 25 (2) 1599-1609 (2009)
10.1149/1.3205696 ©The Electrochemical Society

Role of Lattice Strain and Defect Chemistry on the Oxygen Vacancy Migration at the ($8.3\%Y_2O_3$-ZrO_2) / $SrTiO_3$ Hetero-Interface: A First Principles Study

Akihiro Kushima and Bilge Yildiz

Department of Nuclear Science and Engineering
Massachusetts Institute of Technology, Cambridge, MA, USA

We report on the mechanism and the upper limits in the increase of oxygen ion conductivity at oxide hetero-interfaces, particularly the $8.3\%Y_2O_3$-ZrO_2/$SrTiO_3$ (YSZ/STO) as a model interface. We consider two factors contributing to the increase in ionic conductivity at or near the interface: 1) a favorable strain state to shift and/or change the symmetry of electron energy levels to provide improved charge transfer and mobility. 2) the alteration of the defect chemistry to enhance the density and distribution of oxygen vacancies. First principles and Kinetic Monte-Carlo simulations were performed to identify the atomic-scale nature of the hetero-interface and the oxygen vacancy migration barriers and diffusivity. Our results suggest that the modulation in both the lattice strain and the defect chemistry due to the YSZ/STO interface can enhance the ionic conductivity in YSZ up to six orders of magnitude by reducing the migration barrier and increasing the oxygen vacancy concentration, respectively.

Introduction

There is much interest in decreasing the Solid Oxide Fuel Cell (SOFC) operating temperature to an intermediate-to-low temperature range to improve chemical and mechanical stability and reduce the cost. Enhancing the ionic transport in the electrolyte and cathode materials is a key for this purpose. In recent work, nanoscale hetero-layered structures were shown as means for significantly increasing the transport properties (1-5). The presence of an interface between dissimilar oxides is commonly the source of charged mobile defects and local anisotropic distortions and strained interatomic bonds. These contribute to changes in the local electronic structure; formation, coordination and redistribution of charged defects; and mobility of defects in the vicinity of interfaces. Most recently, an eight order of magnitude increase in ionic conductance for 1-30 nm-thick yttria stabilized zirconia (YSZ) layers coherently "strained" between dielectric $SrTiO_3$ (STO) layers was reported (5). The exact nature of the ionic versus electronic conductance induced in the vicinity of YSZ/STO interface remains debatable. While these observations imply that the hetero-interfaces with controlled lattice-strain and defect-chemistry can play an important role in improving the ionic mobility, results to date remain phenomenological without systematic theoretical efforts supported by experiments.

To understand the underlying mechanism of oxygen anion transport, a number of theoretical studies using atomistic simulation based on both density functional theory

(DFT) and empirical potentials have been conducted (6-8). However, most of them are focused on the "bulk" or the "surface" ionic transport. Some theoretical studies exist for the hetero-interfaces, but only on specific cases, i.e. CaF_2/BaF_2, CeO_2/YSZ (7). A systematic investigation on the effect of hetero-interface structure on the ionic transport mechanisms is still missing.

Our research objective is to elucidate the mechanism and to identify the upper limits in the increase of oxygen ion conductivity in the vicinity of the oxide hetero-interfaces, particularly for the YSZ/STO interface in this work. We consider two main mechanisms contributing to the enhancement at the hetero-interface: 1) a favorable strain state at the interface to shift and/or change the symmetry of electron energy levels to provide for improved charge transfer (9) and improved ion mobility (10), and 2) the alteration of the defect chemistry (11,12) near the interface to enhance the density and distribution of desired charge carriers.

Simulation Approach

To probe the contribution from two mechanisms mentioned above, we evaluated the effect of bond strain on the oxygen migration barrier, and the role of hetero-interface defect chemistry separately in the YSZ/STO problem domain in this work. First, it is important to identify the vacancy-cation interactions to determine the defect distribution in the bulk YSZ. Upon identifying the stable cation-vacancy ordering, the effect of strain on the migration barrier at the local scale and the effective vacancy diffusivity was calculated. Finally, the defect chemistry at the vicinity of the hetero-interface was investigated to clarify how the vacancy formation and distribution is altered with the presence of the interface. We used first principle based simulations to directly and accurately probe the atomistic-scale nature of the vacancy migration and the hetero-interface. Kinetic Monte Carlo method was used for calculating the effective diffusivities.

The first principles calculations were performed using the Vienna *ab initio* simulation package (VASP) (13,14) which employs density functional theory (DFT) using plane-wave basis set. Projector-augmented wave (PAW) method (15,16) with plane waves up to the energy cutoff at 400 eV was used and the exchange-correlation energy was evaluated by generalized gradient approximation (GGA) using Perdew-Burke-Ernzerhof (PBE) function (17). Γ point in the Brillouin zone was selected in the calculation. The same condition was applied to all of the simulations in this study unless stated otherwise.

YSZ has the fluorite crystal structure with cations (Y^{3+}, Zr^{4+}) occupying FCC lattice

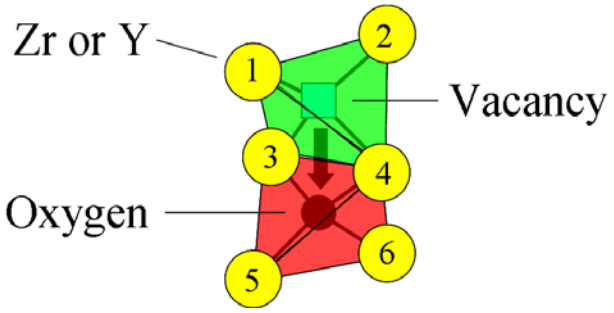

Figure 1. Migration path of the oxygen vacancy.

sites and O^{2-} ions occupying the tetragonal sites. For every two Y atoms, one oxygen vacancy is created to satisfy charge neutrality. The oxygen vacancy migrates by hopping to the adjacent tetragonal site as schematically illustrated in Fig. 1. The migration barrier depends on the neighboring atoms 1-6 in the figure (8). Accounting for the surrounding cations within the larger cutoff radius around the migration path is necessary to accurately quantify the effect of the strain on the migration barrier (18). However, this leads to an impractical number of patterns (well above 10,000 just by including next nearest neighbor cations to the path) to be handled by the DFT simulation. Therefore, here we considered three combinations of atoms at the sites 3 and 4, Zr-Zr, Zr-Y, and Y-Y, in the migration path show in Fig. 1. This approach was validated by Car *et al.*'s work (18), which could capture the trend in ionic conductivity in YSZ as a function of Y_2O_3 doping. Here, we expect that this approximation is also sufficient to capture the quantitative effect of the strain on the ionic conductivity. A database of migration barrier values at different lattice strains was constructed using this approach.

Kinetic Monte-Carlo (KMC) simulations were performed to quantify the impact of strain on the effective oxygen migration. In the simulation model, oxygen atoms were assumed to move to the nearest neighbor oxygen sublattice through the path shown in Fig. 1. The oxygen migrates between two cations in this hopping process. The hopping rate for jumps across the three possible cation patterns (Zr-Zr, Y-Zr, and Y-Y) were obtained by the Boltzman relationship as,

$$\nu_{AB} = \nu_0 \exp\left(\frac{-E_{AB}}{k_B T}\right), \qquad [1]$$

where E_{AB}, found by the DFT simulations, denotes the migration barrier across the A-B cation pair. The attempt frequency was fixed at $\nu_0 = 10^{13}$ s^{-1} which is appropriate for the most metal oxide systems. The periodic boundary conditions were applied to all three dimensions of the simulation cell. The vacancy diffusivity, D_v is extracted from mean square displacement $\langle R^2 \rangle$ calculated in the KMC simulation using the Einstein relation,

$$\langle R^2 \rangle = 6 D_v t \,. \qquad [2]$$

Defect Structure in YSZ: Oxygen Vacancy and Y Cations

We tested various defect configurations for the YSZ model with 30 Zr, 2 Y, and 63 O atoms to determine the favorable vacancy location to Y cations. Here, we chose minimum amount of doping to calculate interaction between the Y atoms and the oxygen vacancy. At this low Y_2O_3 doping (3%), the YSZ oxygen sublattice cannot keep its cubic structure at the local scale (19). Therefore, the atoms outside of the 2nd neighbor cation sites to Y and the 3rd neighbor oxygen sites to the oxygen vacancies were fixed to retain the cubic phase (19).

Figure 2 shows the variation of the total energy with different location of the oxygen vacancy with respect to the Y cation. The result indicates that the vacancies are most likely to exist at the second nearest neighbor oxygen sites to the Y atoms. This result is

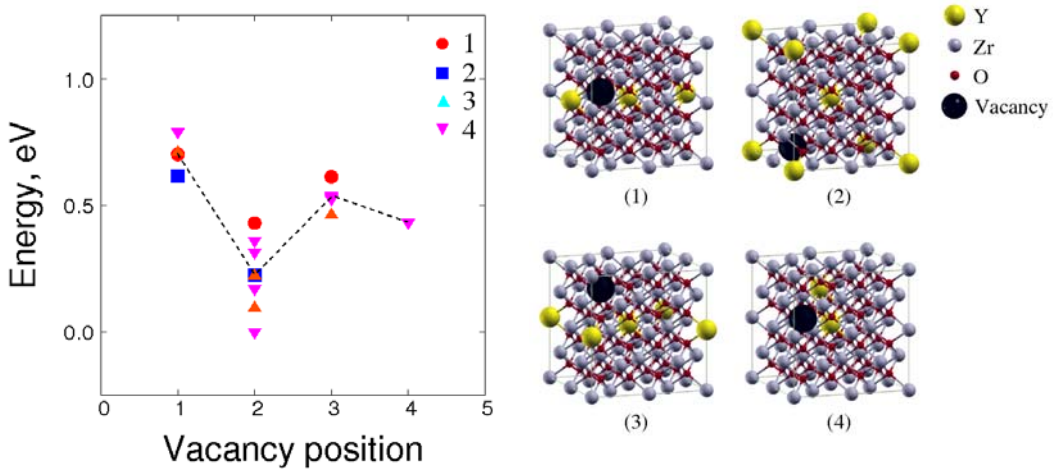

Figure 2. Energy variation with different neighboring location of the oxygen vacancy with respect to the Y cations. The numbers correspond to different distribution of Y atoms in the unit cells shown on the right.

consistent with experimental (20,21) using extended x-ray absorption fine structure and other theoretical studies (8,19) using DFT. Figure 2 also indicates that the total energy can vary by up to 0.5 eV when the Y cation is located at the third or first neighbor to the vacancy, instead of the second. Such large energy difference also suggests that the cation configuration surrounding the diffusion path of the oxygen-vacancy pair should be taken into account for accurate evaluation of the migration barriers.

Effect of Strain on the Oxygen Vacancy Transport

Calculation of the Migration Barrier

The simulation model for calculating the effect of planar lattice strain includes 30 Zr, 2 Y, and 63 O atoms corresponding to 3% Y_2O_3 doping. Only the atoms within the first oxygen neighbor distance to the migrating oxygen-vacancy pair were relaxed, and all the other atoms were restrained in the perfect fluorite lattice sites. This is done to retain the cubic structure and at the same time make the calculations feasible. The planar strain was applied to the structure by elongating the unit cell vectors along the corresponding strain directions. For each combination of the cations, the migration barrier of the paths parallel and perpendicular to the strain direction was calculated. The saddle point corresponded to the diffusing oxygen between site 3 and 4 in Fig. 1. The energy minimization was performed by restricting the three atoms (the two cations at site 3 and 4 and the diffusing oxygen) to relax only within the plane perpendicular to the migration path. The corresponding migration barrier was calculated as the energy difference between the saddle-point energy and the initial state energy. We conducted nudged elastic band calculations (22) to precisely calculate the migration barrier, and confirmed that the results from this simplified procedure were valid.

Figure 3 shows the change in the vacancy migration barrier with respect to the lateral strain for three surrounding atom configurations. The solid and the dashed lines indicate the barriers for the paths parallel and perpendicular to the strain direction, respectively. At zero strain, the migration barrier through cation pairs Zr-Zr, Y-Zr, and Y-Y are 0.56 eV, 0.99 eV, and 2.3 eV, respectively. These results are consistent with the barriers

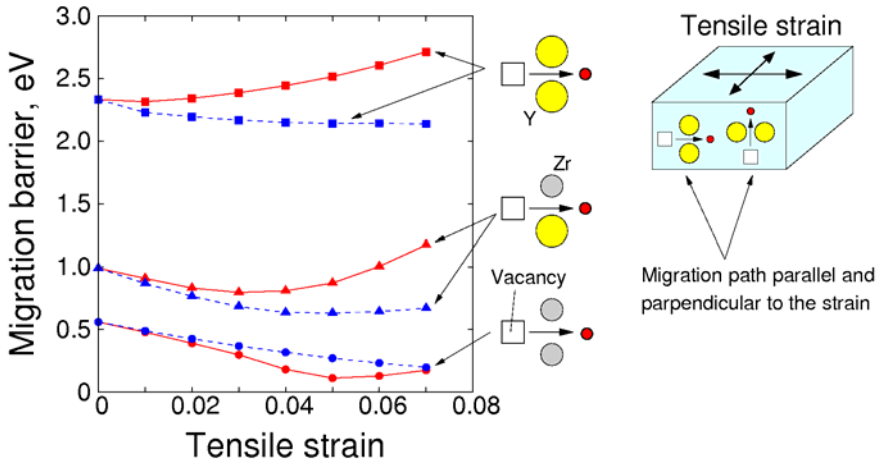

Figure 3. Lattice strain dependence of the energy barrier for oxygen vacancy migration in 3%Y_2O_3-ZrO_2. The solid lines and the dashed lines indicate the barrier along and perpendicular to the strained direction, respectively, as illustrated in the inset.

calculated by Car *et al.* (18) showing the same order of the barrier values; 0.58, 1.29 and 1.86 eV, respectively. The difference can be due to the difference in the Y_2O_3 doping ratios, the corresponding cation environment near the vacancy, and the number of atoms relaxed in the simulation. However, the relative order of the magnitude of the barrier is the same; lowest for Zr-Zr, highest for Y-Y. Therefore, the barriers calculated in this study are expected to represent close-to-accurate values for the quantitative evaluation of the migration process. However, our calculation is underestimating the barrier compared to the experimentally measured diffusion barrier in YSZ of 0.8-1.0 eV (23), and thus, is expected to represent the upper limits in the calculated diffusivity.

As the lattice strain increases, the results show that the migration barriers of the paths parallel to the strain decrease to a minimum value and increase subsequently. The barriers of the paths perpendicular to the strain decreases within the entire calculated strain range except for the path through Y-Zr pair. This implies that there exists an optimum strain that could maximize the ionic diffusivity, and that there must be competing factors increasing and decreasing the barrier. Decreasing of the barrier with increasing strain at low strain values is expected because the distance between the two cations in the path

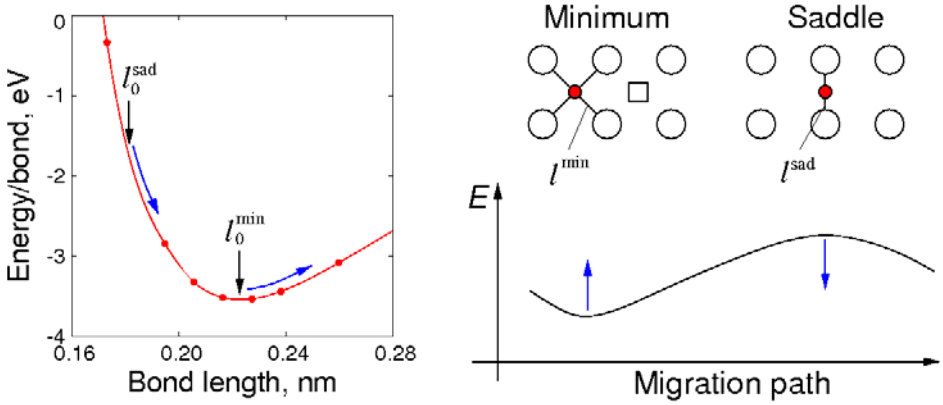

Figure 4. Change in average energy/bond in the simulation cell as a function of the Zr-O bond length in ZrO_2. l^{min} and l^{sad} are the bond lengths between the diffusing oxygen and the 1st neighbor cations, and l_0^{min} and l_0^{sad} in (a) correspond to $\varepsilon = 0.00$ in the YSZ.

(both parallel and perpendicular to the strain) increases with strain opening the channel for the migration. Figure 4a shows the change in the system energy with respect to Zr-O bond length in ZrO_2. l^{min} and l^{sad} denote bond lengths between the diffusing oxygen and its 1st neighbor Zr cation, respectively. Here, we assume that the minimum and the saddle energies are mainly governed by l^{min} and l^{sad}. Because both l^{min} and l^{sad} increase with increasing strain, the minimum energy increases and the saddle point energy decreases (blue arrows in Fig. 4a) resulting in the reduction of the migration barrier height as schematically shown in Fig. 4b. On the other hand, the increase in the barrier arises because of the larger distortion of oxygen sub-lattice near the migration path at higher strain states. Figure 5 shows the minimum- and saddle-point atom configurations for ε = 0.00 and 0.05 for the Zr-Zr at sites 3 and 4. At ε = 0.00, the oxygen that is most displaced during the migration process is the diffusing oxygen itself, and the other 1st neighbor oxygen atoms to the vacancy are shifted only slightly. At ε = 0.05, the two oxygen atoms indicated by the solid circles distorts largely away from the fluorite oxygen sublattice sites toward the vacancy. When the diffusing oxygen migrates to replace the vacancy, the two oxygen atoms are also subject to large displacement. The same type of distortion was found for all the other cation combinations at sites 3 and 4. This collective motion of oxygen atoms could be the main factor contributing to the increase in the activation barrier at higher strain. To explain the disorder effect more quantitatively, the migration barrier across two Zr-Zr cation pair was calculated by relaxing all the atoms in the simulation cell at ε = 0.00, and compared to the value in Fig. 3. In this calculation, oxygen anions randomly displaced from their fluorite lattice site while keeping an overall cubic structure, consistent with theoretical and experimental results reported in references 19, 24, and 25. This procedure lead to a higher migration barrier, 1.1eV, compared to 0.56eV obtained from the model with limited relaxation and distortion of atoms. This result depicts that the distortion of the oxygen sublattice is the source of the increased barrier at higher strain. However, for the computational efficiency we limited the calculations thus far to the simplified model. Note that this could lead to obtaining the upper limit of the effect of the strain since the barrier is underestimated by not considering the long-range distortion of the oxygen sublattice.

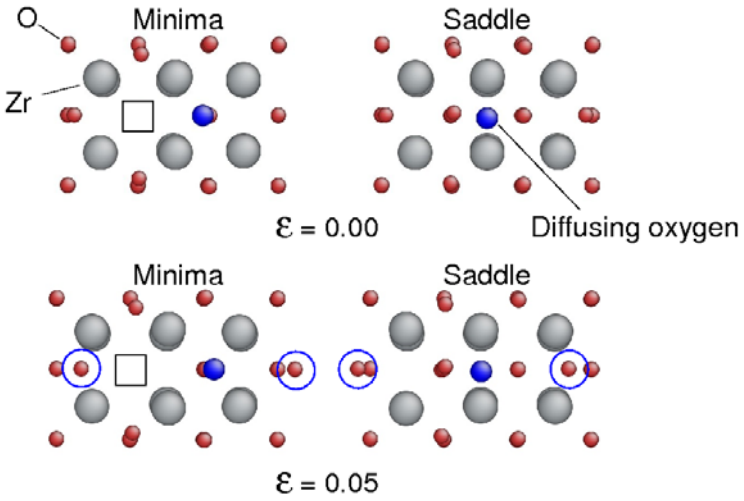

Figure 5. The initial and the saddle point configurations of the oxygen vacancy migrating parallel to the strain direction at ε = 0.00 and 0.05, for both atoms in the migration edge as Zr. For ε = 0.05 more oxygen atoms (indicated by solid circles) are involved in diffusion process.

Kinetic Monte-Carlo (KMC) Simulations of the Oxygen Vacancy Diffusion

To quantify the overall impact of the lattice strain on the effective ionic conductivity, Kinetic Monte-Carlo (KMC) calculations were performed, using the migration path configurations and barrier energies discussed above. YSZ model had a 10×10×10 cubic fluorite lattice containing 4000 cation sites and 8000 oxygen sites. Y atoms and the vacancies were placed randomly at the cation and the oxygen sites, respectively, corresponding to a 8.3 % Y_2O_3 doping ratio. Oxygen vacancy diffusivity, $D_{v,}$ was calculated for biaxial lattice strains from 0.00 to 0.07, and at temperatures 400 – 1000K, using the migration barriers shown in Fig. 3.

Figure 6a presents the resulting behavior of vacancy diffusion constant, D_v, as a function of strain and temperature. The vacancy diffusivity increases with strain, and reaches its maximum at $\varepsilon = 0.05$. The effective migration barrier shown in Fig. 6b was obtained by fitting the temperature dependence of the diffusivity by the Arrhenius law at different strains. The effective barrier shows the minimum at $\varepsilon = 0.05$ corresponding to the maximum effective diffusivity. When compared to Fig. 3, the result shown in Fig. 6b suggests that the dominating diffusion path has Zr-Zr at sites 3 and 4 in Fig. 1.

The increase in the diffusivity with strain is more significant for the lower temperatures. Nearly six orders of magnitude higher diffusivity is expected at 400 K with $\varepsilon = 0.05$. This significant increase is close to the magnitude of enhancement in the ionic conductivity at the YSZ/STO hetero-interface reported by Barriocanal *et al.* (5). Note that the calculated enhancement in the diffusivity here could serve as an upper-limit estimate for the effect of strain, because only the local atom relaxation in the migration process was considered. While the relaxation of the surrounding cations should be accounted for a more accurate estimate, our results imply the potential of the strain to drastically enhance the ionic conductivity in YSZ.

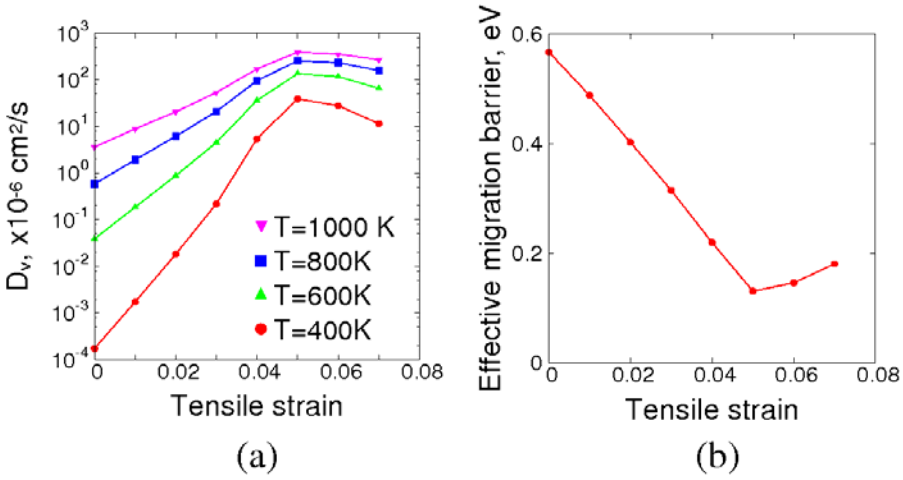

Figure 6. (a) Vacancy diffusion constant, D_v calculated by KMC method, for 8.3%Y_2O_3-ZrO_2. The diffusivity increases with tensile strain up to ε=0.05, and decreases subsequently. The increase is more significant at lower temperatures, and nearly six orders of magnitude of raise at T=400 K. (b) Effective migration barrier as a function of the applied strain. The lowest barrier is observed at $\varepsilon = 0.05$, consistent with results in (a).

Defect Chemistry at the Vicinity of the Hetero-Interface

The charged defect density and distribution, particularly that of the oxygen vacancies, at and near the interface is another mechanism that we considered to elucidate the origin of the high ionic conductivity at the ZrO_2/STO hetero-layered structure. The enrichment of defects near the interface is known to affect the ionic conductivity due to the space-charge effect (26), another important factor to be considered.

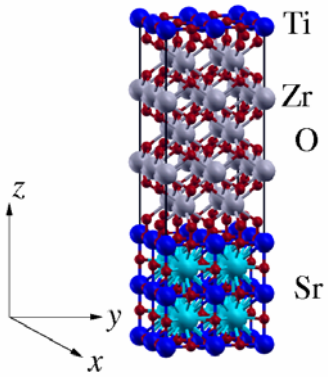

Figure 7. Simulation model of the ZrO_2/STO layered structure.

Here we present two models for the ZrO_2/STO hetero-layer structure to identify the possible mechanisms through which an enhancement in ionic conductivity in ZrO_2 could be achieved due to oxygen vacancy formation and distribution. In the first model, the interface oxygen atoms are aligned with those on TiO_2 plane of STO. This is the structure shown in the experimental observation in (5). A subset of vacancy distribution schemes is considered near the ZrO_2/STO hetero-interface model with a 1.5nm-thick ZrO_2 layer.

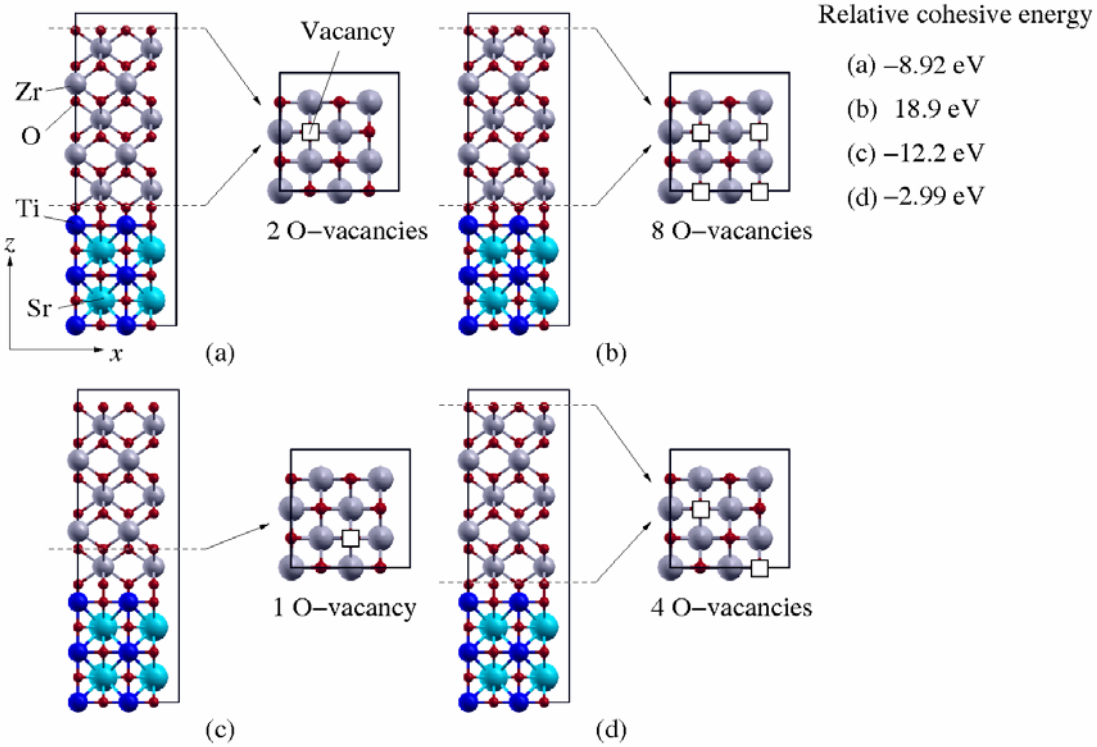

Figure 8. Four different configurations for the location of the oxygen vacancy, and their cohesive energies relative to the structure without any vacancies.

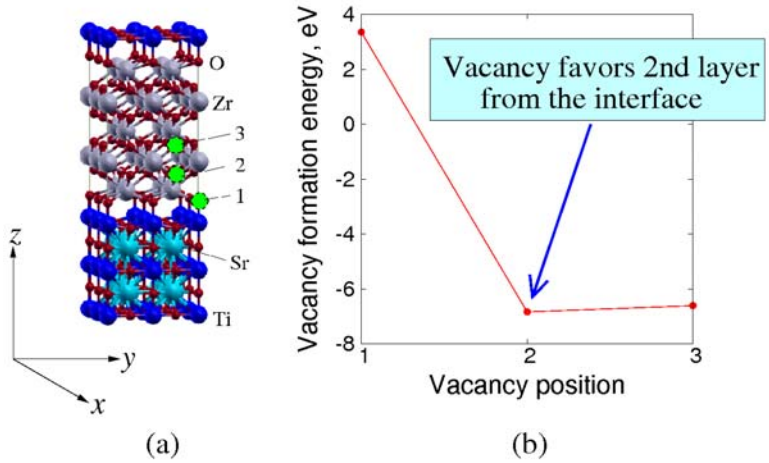

(a) (b)

Figure 9. (a) Simulation model of ZrO_2/STO interface with oxygen atoms on the oxygen sites of the SrO-termination layer on STO. The green circles indicate the vacancy positions considered in the calculations here. (b) The vacancy formation energy of the configurations with the vacancy locations indicated in (a).

The model contains 12 Ti, 8 Sr, 20 Zr, and 80 O atoms, as shown in Fig. 7. In this configuration, eight oxygen atoms need to be removed to maintain overall charge balance in the simulation cell. The stability of the structure with different distributions of the vacancies was compared. Fig. 8 shows the sub-set of configurations considered here; (a) two vacancies (one at each interface), (b) eight vacancies (4 at each interface), (c) one vacancy at the second oxygen layer from the interface, and (d) four vacancies (two at each interface). The cohesive energies relative to the structure without any vacancies are shown for comparison. The result indicates that the configuration with all the eight vacancies located at the interface is the least stable. On the other hand, the presence of the oxygen vacancy at the second layer into the ZrO_2 nanolayer from the interface is the most stable among these configurations.

The second ZrO_2/STO model had the interface oxygen atoms located at the oxygen sites of the SrO-termination layer on STO. We note that the cohesive energy of the first model is lower than that of the second model by about 5 eV. The model consisted of 12 Ti, 8 Sr, 20 Zr, and 72 O atoms as indicated in Fig. 9a with the periodic boundary conditions applied to all three dimensions. In this model, the charge balance is maintained without having to remove any oxygen atoms. One vacancy was imposed by removing an oxygen atom from the 1st, 2nd, and 3rd oxygen layers into the ZrO_2 from the STO interface, as shown in Fig. 9(a). The comparison of the vacancy formation energies of these three cases suggests that a single oxygen vacancy is favored to form at the second layer from the interface, rather than at the ZrO_2/STO interface.

Results from both models presented here suggest that the vacancies could extend into the ZrO_2 layer, inducing a higher vacancy concentration and in principle ionic conductance *within* the ZrO_2 nano-layer even in the absence of Y_2O_3 doping.

Relative Contributions of Strain and Defect Chemistry to Ionic Conductivity Increase

The oxygen self-diffusivity, D_O, is defined by considering the jump balance as,

$$D_O = \frac{c_v}{1-c_v} D_v \qquad [3]$$

where c_v is the vacancy concentration fraction. Ionic conductivity increases by an increase in vacancy concentration. For the 1.5-nm-thick model, 8 out of 64 oxygens in ZrO_2 layer are removed, creating ionic conductance even without the Y_2O_3 doping. This corresponds to the increase in vacancy concentration by nearly 15 %, a value greater than the 8% vacancy concentration in an 8.3% Y_2O_3 doped YSZ. This leads to a 23% vacancy concentration for the ZrO_2 in the YSZ/STO layered structure. Assuming that presence of additional vacancies does not alter the migration barrier, the oxygen self-diffusivity in ZrO_2 layer as part of the hetero-layered structure is expected to be three times larger than the bulk ZrO_2, from Eq.3. The enhancement in the oxygen diffusivity due to the increasing vacancy concentration is scaled by $c_v/(1-c_v)$ which scales almost linearly at low c_v. Therefore, a linear increase in ionic conductivity is expected due to the defect chemistry. While this is important, linear dependence is small compared to the exponential contribution from the reduced migration barrier as a result of lattice strain.

Conclusion

In this study, we have demonstrated that both the lattice mismatch-induced strain and the altered defect chemistry due to the YSZ/STO interface can significantly contribute to the increase in the ionic conductivity. The lattice strain directly reduces the migration barrier, and thus, leads up to six orders of magnitude increase in ionic conductivity at 400 K in YSZ. On the other hand, the introduction of the YSZ/STO interface alters the defect chemistry increasing the vacancy concentration within the ZrO_2 layer. This effect leads to an approximately linear contribution to increase the ionic conductivity of ZrO_2 in the hetero-layered structure. However, the lattice mismatch-induced strain is expected to have a dominating and exponential contribution due to the reduction of the vacancy migration barrier.

References

1. N. Sata, K. Eberman, K. Eberl and J. Maier, *Nature*, **408**, 946 (2000).
2. T. Suzuki, I. Kosacki, and H. U. Anderson, *Solid State Ionics* **151**, 111 (2002).
3. X. X. Guo, I. Matei, J. -S. Lee, and J. Maier, *Appl. Phys. Lett.* **92**, 103102 (2007).
4. I. Kosacki, C. M. Rouleau, P. F. Becher, J. Bentley, and D. H. Lowndes, *Solid State Ionics* **176**, 1319 (2005).
5. J. G-. Barriocanal, A. R-. Calzada, M. Varela, Z. Sefrioui, E. Iborra, C. Leon, S. J. Pennycook, and J. Santamaria, *Science* **321**, 676 (2008).
6. A. K. Ivanov-Shitz, *Crystallogra. Rep.* **52**, 129 (2007).
7. D. C. Sayle, J. A. Doig, S. C. Parker, and G. W. Watson, *Chem. Commun.*, 1804 (2003).

8. R. Pornprasertsuk, P. Ramanarayanan, C. B. Musgrave, and F. B. Prinz, *J. Appl. Phys.* **98**, 103513 (2005).
9. M. Mavrikakis, P. Stoltze, and J. K. Nørskov, *Catal. Lett.* **64** (2000), 101.
10. J. Kilner, *Nature Materials*, **7** (2008), 838.
11. J. Maier, *Prog. in Solid St. Chem.* **23** (1995), 171.
12. X. X. Guo, I. Matei, J. -S. Lee, and J. Maier, *Appl. Phys. Lett.* **91**, 103102 (2007).
13. G. Kresse and J. Hafner, *Phys. Rev*. B **47**, 558 (1993).
14. G. Kresse and J. Furthmüller, *Phys. Rev.* B **54**, 11169 (1996).
15. P. E. Blöchl, *Phys. Rev.* B **50**, 17953 (1994).
16. G. Kresse and D. Joubert, *Phys. Rev.* B **59**, 1758 (1998).
17. J. P. Perdew, K. Burke, and M. Ernzerhof, *Phys. Rev. Lett.* **77**, 3865 (1996).
18. R. Krishnamurthy, Y. -G. Yoon, D. J. Srolovitz, and R. Car, *J. Am. Ceram. Soc.*, **87**, 1821 (2004).
19. G. Stapper, M. Bernasconi, N. Nicoloso and M. Parrinello, *Phys. Rev.* B **59**, 797 (1999).
20. P. Li, I- W. Chen, J. E. Penner-Hahn, *Phys. Rev* B **48**, 10074 (1993).
21. D. Komyoji, A. Yoshiasa, T. Moriga, S. Emura, F. Kanamaru and K. Koto, *Solid State Ionics* **50**, 291 (1992).
22. G. Mills and H. Jónsson, *Phys. Rev. Lett.* **72**, 1124 (1994).
23. M. Kilo, C. Argirusis, G. Borchardt, and R. Jackson, *Phys. Chem. Chem. Phys.* **5**, 2219 (2003).
24. S. Ostanin, E. Salamatov, A. J. Craven, D. W. McComb, and D. Vlachos, *Phys. Rev.* B **66**, 132105 (2002).
25. C. Pascal and P. Duran, *J. Am. Ceram. Soc.* **66**, 23 (1986).
26. J. Maier, *Prog. Solid St. Chem.* **23**, 171 (1995).